Physical Modeling of Hot-Carrier Degradation for Short- and Long-channel MOSFETs

Stanislav Tyaginov*,•, Markus Bina*, Jacopo Franco°, Dmitri Osintsev*, Oliver Triebl*,†, Ben Kaczer°, and Tibor Grasser*
*Institute for Microelectronics, Technische Universität Wien, 1040 Vienna, Austria
•A.F. Ioffe Physical-Technical Institute, 194021 Saint-Petersburg, Russia
°imec, Kapeldreef 75, B-3001 Leuven, Belgium
†Global TCAD Solutions, 1010 Vienna, Austria
Email: tyaginov@iue.tuwien.ac.at

***Abstract*—We present the first physics-based model for hot-carrier degradation which is able to capture degradation in both short- and long-channel SiON nMOSFETs. Degradation is considered to be due to the breaking of Si-H bonds at the SiON/Si interface. Contrary to previous modeling attempts, our approach now correctly considers the intricate superposition of multivibrational bond excitation and bond rupture induced by a solitary hot carrier based on experimentally confirmed distributed activation energies. All processes are treated as competing pathways, leading to bond dissociation from all vibrational levels. These rates are determined by the carrier acceleration integral and by the bond energetics. The acceleration integral is calculated using the carrier energy distribution. Corresponding distribution functions are found by a thorough solution of the Boltzmann transport equation. We demonstrate that electron-electron scattering plays the dominant role. As for the bond energetics, we consider the dispersion of the activation energy as well as its reduction induced by the interaction of the bond dipole moment with the electric field. All the model ingredients are incorporated into the same simulation framework based on the deterministic solver of the Boltzmann transport equation, ViennaSHE.**

***Index Terms*—hot-carrier degradation, physics-based model, deterministic Boltzmann transport equation solver, MOSFET, interface traps.**

I. Introduction

Hot-carrier degradation (HCD) is a highly complex phenomenon, which involves a wide hierarchy of physical effects. This hierarchy connects the microscopic level of defect generation with the device physics level [1–4]. HCD is widely adopted to be due to the dissociation of passivated Si-H bonds at or near the dielectric/semiconductor interface. This dissociation is induced by the charge carriers in the channel which interact with the bonds. The efficiency of such an interaction is defined by energies deposited at the interface by carriers from the ensemble moving through the device. Therefore, the crucial link in the aforementioned hierarchy between the device and microscopic levels is the carrier transport treatment, which is essential for a proper capture of bond-breakage kinetics as well as for modeling of the degraded transistors. Thus, an adequate description of carrier transport based on the thorough solution of the Boltzmann transport equation (BTE) is expected to be the central aspect of any physics-based hot-carrier degradation model. These considerations already reflect the complexity

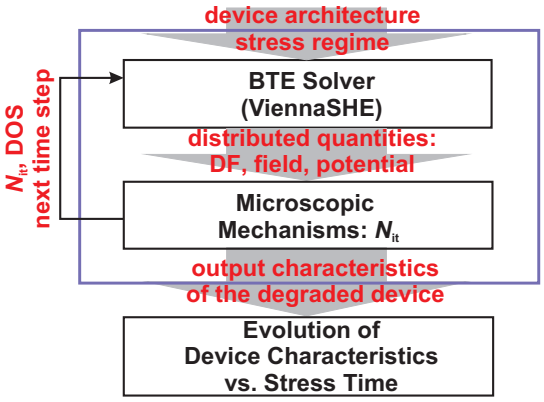

Fig. 1: The schematic representation of the model structure. The model is incorporated into the Boltzmann transport equation solver ViennaSHE. The ViennaSHE framework allows to consider all the aspects of the problem consistently, namely carrier transport, the kinetics of defect generation, and modeling of the degraded devices.

of the HCD problem, which can be therefore separated into three subtasks: (*i*) carrier transport treatment by solving the Boltzmann transport equation (BTE), (*ii*) description of defect generation kinetics at the microscopic level, and (*iii*) modeling of the degraded devices, see Fig. 1 [4, 5].

In practice, however, due to the complexity of HCD, this detrimental phenomenon is very often modeled at an empirical level [6–8]. The corresponding models are of very limited validity, because under different stress/operating conditions and/or device topologies different mechanisms can dominate HCD. For instance, electron-electron scattering (EES) was claimed to be of key importance in ultra-scaled devices [9, 10]. EES substantially reinforces HCD for devices fabricated in the 180 nm node and below. This scattering mechanism also determines the HCD temperature behavior in nano-scale transistors [2, 11]. Another conceptual peculiarity is the change of the dominant mechanism of hot-carrier degradation which accompanies MOSFET miniaturization. In long-channel and/or high-voltage MOSFETs HCD is triggered by hot carriers. Within this process one of the bonding electrons is excited to an antibonding (AB) state, which makes the entire bond unstable, and hence leads to its rupture [12]. Carrier energies

978-1-4799-3317-4/14/$31.00 ©2014 IEEE

in the ensemble are high enough to induce a bond-breakage event in a single collision. This process is termed as the AB-mechanism. At the same time, if operating voltages are scaled down such energetical electrons are not likely. However, as was reported in [13] HCD can be severe even in ultra-scaled MOSFETs. The reason behind this is that the ensemble of "colder" carriers can induce a multiple vibrational excitation (MVE) of the bond. Such an excited bond is more likely to be broken by a single carrier. At the device level, this alteration of the dominant bond dissociation mechanism was shown to be responsible for the shift of the worst-case HCD conditions in ultra-scaled devices as compared to long-channel transistors [2, 14, 15]. Therefore, the change of the physical picture behind hot-carrier degradation may also dramatically impact the device life-time, thereby making empirical models non-predictive.

In order to avoid the complicated solution of the BTE while still capturing the main mechanisms contributing to HCD, simplified schemes based on the "energy driven paradigm" proposed by Rauch and LaRosa [10, 16] are commonly used [17, 18]. The energy driven paradigm relates the defect generation rate to the stress/operating voltages via so-called characteristic "knee energies". One of the most successful HCD models, the Bravaix model, is designed in the same fashion [17, 19]. This approach identifies three main modes governed by the AB-, EES, and MVE-processes. This consideration, however, is problematic because all these components act as scattering mechanisms, thereby affecting carrier transport, and as a result the bond dissociation rate. Therefore, these mechanisms need to be considered consistently.

Furthermore, although the importance of EES has been acknowledged, EES is usually omitted since it is very difficult to model, leading to contradictory claims [18, 20]. For instance, the authors of [18] report that the role of EES is overestimated and that instead a two-particle process dominates HCD. Finally, in spite of the fact that it has been suggested that a superposition of AB- and MVE-mechanisms has to be considered [1], they are typically approximated as being independent [17, 21]. Also, although the Bravaix model considers a particular superposition of these process called as the two-particle process [17], it would be worth to incorporate the vibrational excitation of the bond to an arbitrary level followed by hydrogen release. In the previous version of our HCD model [4, 21] we considered the AB- and MVE-processes weighted with some empirical factors which were fitting parameters of the model. Such a description is physically doubtful because these mechanisms are just different pathways of the same bond dissociation reaction and have to be treated consistently as competing processes within the same equation framework.

The main goal of this work is to develop and validate a physics-based model for hot-carrier degradation which incorporates the interaction between the AB- and MVE-mechanisms. As an essential ingredient of carrier transport, EES is consolidated into the model. We also consider the statistical variations of the bond-breakage energy and the interaction between the dipole moment of the bond and the electric field. We thoroughly analyze the contributions of all the model ingredients to hot-carrier degradation.

II. Experiment

To properly assess the validity of the model, we employ short- and long-channel nMOSFETs with SiON films (EOT = 2.5 nm) grown by a decoupled plasma nitridation process with L_{G} = 65 nm and 150 nm. We intentionally did not use transistors with novel high-K gate dielectrics in order to avoid intensive charge trapping in the oxide bulk. Therefore, employing the SiON material as a gate insulator was the most reasonable choice in this context. Both transistor types were subjected to hot-carries stress in their respective worst-case regimes, i.e. at $V_{\mathrm{gs}} = V_{\mathrm{ds}}$ and $V_{\mathrm{gs}} \sim V_{\mathrm{ds}}/2$ [15, 22]. Since we were not sure that the longest MOSFET behaves as a long-channel device, the substrate current I_{sub} was measured as a function of V_{gs} at a fixed V_{ds}. The I_{sub} maximum was observed at V_{gs} = V_{ds}/2, which is consistent with a long-channel behavior.

The device architecture was obtained using the Sentaurus process simulator based on the imec process flow, while the device characteristics were obtained using ViennaSHE. Both process and device simulators were calibrated in a fashion to represent electrical characteristics of the fresh MOSFET. This calibration is an important step allowing to reliably simulate doping profiles which are of key importance in the context of carrier transport.

To demonstrate the impact of the main model ingredients on HCD we used two different drain voltages, V_{ds} = 1.8 and 2.2 V (linked to V_{gs} via the worst-case conditions). The devices were stressed for ∼10 ks at room temperature and the linear drain current ΔI_{dlin} degradation was measured to assess HCD. We intentionally used short- and long-channel devices and stressed them at high voltages to efficiently trigger the dominant degradation mechanisms. This strategy was expected to help performing a careful analysis of contributions of all the model ingredients.

III. The Model

Our physics-based HCD model is implemented in the deterministic BTE solver ViennaSHE [20, 23]. ViennaSHE calculates carrier energy distribution functions (DFs) for a particular device architecture and bias condition (see Fig. 2) as well as other macroscopic quantities, e.g. the electric field, Fig. 3. This information is then used to calculate the carrier acceleration integrals (AIs) which define the bond dissociation rates from each level E_i of the bond vibrational modes [1]:

$$I_{\mathrm{AB},i} = \int f(E)g(E)\sigma_0(E - E_{\mathrm{a}} + E_i)^p v(E)\mathrm{d}E, \quad (1)$$

where $\sigma_0(E - E_{\mathrm{a}} + E_i)^p$ is the Keldysh-like reaction cross section [1, 21, 24], E_{a} the activation energy of bond dissociation, and E_i the position of the ith energy level. The carrier DF is denoted as $f(E)$, $g(E)$ is the density-of-states, and v is the carrier group velocity. For the AB-mechanism the factor $p = 11$ is used, while for the MVE-process $p = 1$.

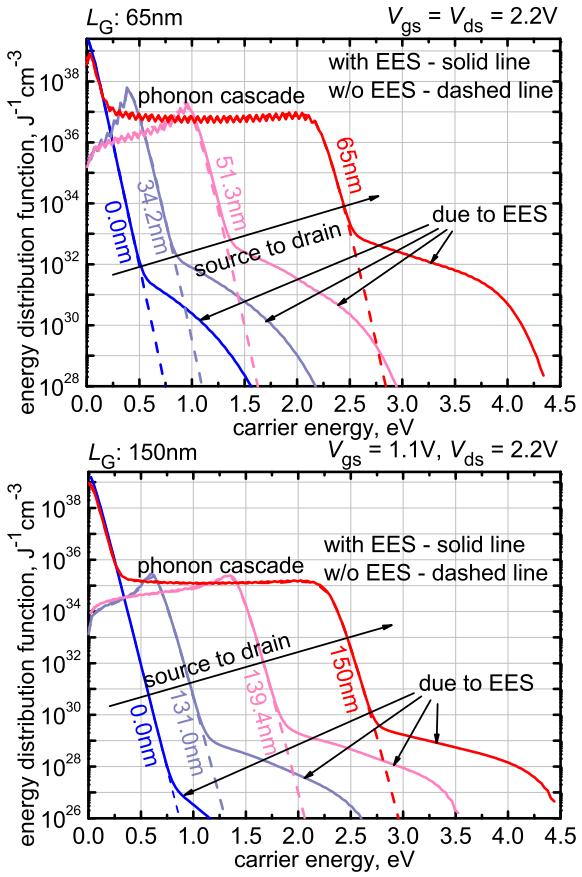

Fig. 2: The carrier energy distribution functions calculated for both 65 and 150 nm devices for $V_{\rm gs} = V_{\rm ds} = 2.2$ V and $V_{\rm gs} = 1.1$ V, $V_{\rm gs} = 2.2$ V, respectively. To see the effect of EES on the DFs the calculations have been performed regarding and disregarding EES. One can see that this scattering mechanism changes the shape of the DFs populating the high-energy tails.

The formula (1) shows that if bond dissociation occurs from the intermediate level i, the barrier is lowered by the corresponding energy E_i. This is realized if first the bond is

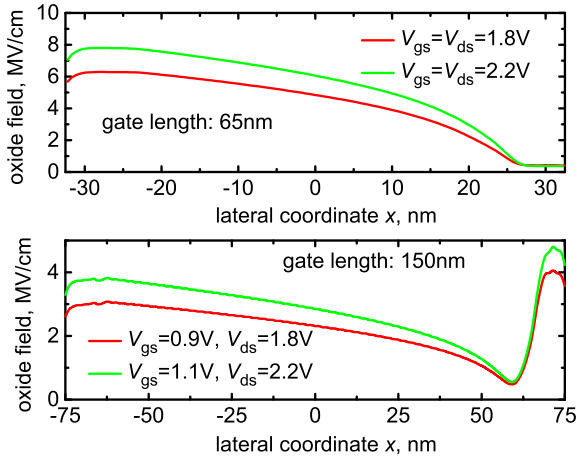

Fig. 3: The oxide electric field as a function of the lateral coordinate x plotted for both 65 and 150 nm MOSFETs and both stress conditions. In all cases the electric field demonstrates a maximum near the source edge of the gate electrode.

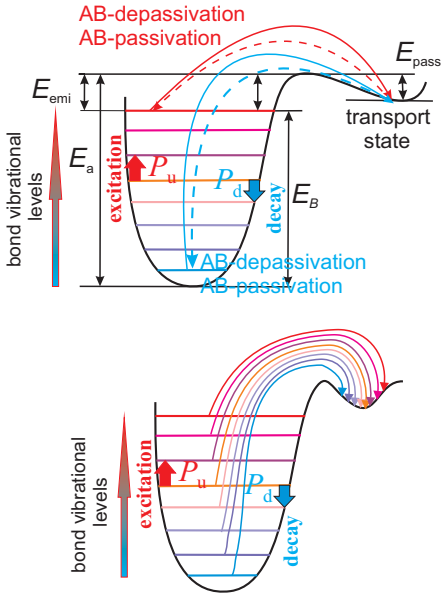

Fig. 4: The Si-H bond as a truncated harmonic oscillator. In previous HCD models only hydrogen release from the ground and last bonded levels has been considered. In the current version of the model we incorporate all possible combinations of MVE- and AB-mechanisms. That means that the bond can first be excited to an intermediate level i by several colder carriers and then dissociated by a solitary high energetical particle.

excited to this level by the MVE-process which is followed by the AB-mechanism, Fig. 4. In other words, a subsequent bombardment of the bond by a series of "colder" carriers eventually excites the bond to an intermediate level i. If then a high energetical carrier collides with the bond, it can trigger the AB-process, thereby leading to hydrogen release. This situation is more general as compared to the previous models [15, 21] where hydrogen release from either the ground state (so-called single-carrier process) or the last bonded level (multiple-carrier process) has been considered, see Fig. 4. Therefore, bond heating via the MVE-process and hydrogen release triggered by the AB-mechanism naturally emerge as *competing pathways of the same reaction*.

To extend the model, we include the terms representing bond passivation/depassivation rates to/from all the eigenstates into the system of rate equations:

$$\begin{aligned}
\frac{{\rm d}n_0}{{\rm d}t} &= P_{\rm d} n_1 - P_{\rm u} n_0 - R_{{\rm a},0} n_0 + R_{{\rm p},0} N_{\rm it}^2 \\
\frac{{\rm d}n_i}{{\rm d}t} &= P_{\rm d}(n_{i+1} - n_i) - \\
&\quad - P_{\rm u}(n_i - n_{i-1}) - R_{{\rm a},i} n_i + R_{{\rm p},i} N_{\rm it}^2 \\
\frac{{\rm d}n_{N_l}}{{\rm d}t} &= P_{\rm u} n_{N_{l-1}} - P_{\rm d} n_{N_l} - R_{{\rm a},N_l} n_{N_l} + R_{{\rm p},N_l} N_{\rm it}^2,
\end{aligned} \tag{2}$$

here $P_{\rm u}/P_{\rm d}$ are rates corresponding to the Si-H bond vibrational mode excitation and decay, while $R_{{\rm a},i}$ and $R_{{\rm p},i}$ are bond rupture and passivation rates with the ith level involved. Oscillator occupation numbers are designated as n_i and N_l is the index for the last bonded state.

The bond dissociation rates $R_{\rm a,i}$ are calculated as

$$R_{{\rm a},n_i} = w_{\rm th} \exp\left[-\left(E_{\rm a} - E_i\right)/k_{\rm B}T\right] + I_{{\rm AB},i}, \tag{3}$$

where the first Arrhenius term describes the hydrogen thermal excitation from a bonded state to the transport mode (with the corresponding attempt frequency $w_{\rm th}$), while the second term is the carrier AI and represents the hot carrier contribution to HCD. As for the bond excitation/deexcitation rates $P_{\rm u}/P_{\rm d}$, they are also expressed via the acceleration integral:

$$\begin{aligned} P_{\rm u} &= I_{\rm MVE} + \omega_{\rm e}\exp\left(-\hbar\omega/k_{\rm B}T_{\rm L}\right), \\ P_{\rm d} &= I_{\rm MVE} + \omega_{\rm e}, \end{aligned} \tag{4}$$

where $\omega_{\rm e}$ is the reciprocal phonon life-time, while $\hbar\omega$ the distance between the oscillator levels.

The system (2) can be solved by applying a time scale hierarchy, i.e. the fact that oscillator transitions are characterized by much shorter time constants than passivation/depassivation processes. As such, the system of $N_{\rm l}$ equations is reduced to the single equation:

$$\frac{{\rm d}N_{\rm it}}{{\rm d}t} = \left(N_0 - N_{\rm it}\right)\Re_{\rm a} - N_{\rm it}^2\Re_{\rm p}, \tag{5}$$

where N_0 is the concentration of precursors, i.e. of the virgin Si-H bonds. $\Re_{\rm a}$ is the cumulative bond-breakage rate, which is just a sum of bond-breakage rates from each individual level weighted with the population number of the level:

$$\Re_{\rm a} = \frac{1}{k}\sum_i R_{{\rm a},i}\left(\frac{P_{\rm u}}{P_{\rm d}}\right)^i, \tag{6}$$

while $\Re_{\rm p}$ is the total passivation rate onto each eigenstate. However, without loss of generality one may represent the $\Re_{\rm p}$ rate by the Arrhenius term for thermal activation over a single barrier, i.e. $\Re_{\rm p} = \nu_{\rm p}\exp(-E_{\rm p}/k_{\rm B}T_{\rm L})$.

$$\begin{aligned} N_{\rm it}(t) &= \frac{\sqrt{\Re_{\rm a}^2/4 + N_0\Re_{\rm a}\Re_{\rm p}}}{\Re_{\rm p}}\frac{1-f(t)}{1+f(t)} - \frac{\Re_{\rm a}}{2\Re_{\rm p}}, \\ f(t) &= \frac{\sqrt{\Re_{\rm a}^2/4 + N_0\Re_{\rm a}\Re_{\rm p}} - \Re_{\rm a}/2}{\sqrt{\Re_{\rm a}^2/4 + N_0\Re_{\rm a}\Re_{\rm p}} + \Re_{\rm a}/2}\times \\ &\quad\times\exp\left(-2t\sqrt{\Re_{\rm a}^2/4 + N_0\Re_{\rm a}\Re_{\rm p}}\right). \end{aligned} \tag{7}$$

Another important model ingredient is the dispersion of the activation energy of bond dissociation. Considering such statistical variations can substantially change the characteristics of the degraded devices simulated with the model. Following [25], we assume that the energy $E_{\rm a}$ obeys a normal distribution with the mean value and the standard deviation of $\langle E_{\rm a}\rangle$ = 1.5 eV and $\sigma_{\rm E}$ = 0.15 eV, respectively. These values are in good agreement with the results of electron-spin resonance studies [26] and with our own findings based on charge-pumping signal analysis [27]. The effect of the activation energy dispersion was incorporated in the manner that the range $[\langle E_{\rm a}\rangle - 3\sigma_{\rm E}; \langle E_{\rm a}\rangle + 3\sigma_{\rm E}]$ was discretized and for each discretization point we evaluated the interface trap density profile $N_{\rm it}(x)$ according to (7) weighted with the Gaussian distribution. Note that – among other things – the fluctuating energy affects the rates $\Re_{\rm a}$ entering both terms in (3), in particular the carrier acceleration integral, see (1).

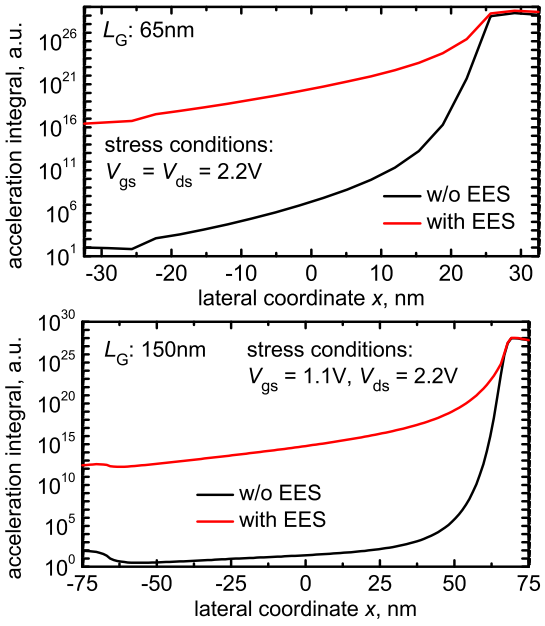

Fig. 5: The carrier acceleration integrals evaluated for both devices and the same stress conditions as Fig. 2. These integrals have been calculated with and without EES. One can see that the effect of EES on the AIs is pronounced in both cases.

It is important to emphasize that one may consider the situation with Si-H bonding energy dispersion in the studied devices in terms of a statistical ensemble. In fact, the concentration of the passivated Si-H bonds is $\sim 10^{12}$ cm^{-2}. The width of the used devices is $W = 10\,\mu$m. In the shortest MOSFET with the gate length of $L_{\rm G}$ = 65 nm the total number of passivated bonds is estimated as $\sim 10^4$. This amount of precursors allows us to treat the fluctuations of the activation energy in terms of continuous distributions. Note that even in the case of W = 100 nm the number of passivated bonds is $\sim$100 and this statistical description is still applicable.

Last but not least important factor which results in variations in the bond dissociation energy is the interaction between the oxide electric field and the dipole moment of the bond [28, 29]. This interaction was reported to be responsible for two different time slopes of HCD [30, 31] and also impacts the intimately related phenomenon of bias temperature instability [32]. We model this effect in the same fashion as proposed in [28] and [29]. The activation energy reduction due to this effect is expressed as the product of the bond dipole moment and the electric field $d \times E_{\rm ox}$.

IV. Results and Discussion

The model is validated by fitting the measured relative change of the linear drain current $\Delta I_{\rm dlin}(t) = |I_{\rm dlin}(t) - I_{\rm dlin}(t=0)|/\Delta I_{\rm dlin}(t=0)$ (i.e. normalized with the respect the current of the fresh transistor) for both devices and both stress conditions using the *same set of model parameters*. Since the devices are stressed at high $V_{\rm ds}$, the AB-mechanism was expected to play a major role. This is confirmed by Fig. 2 where the carrier distribution functions calculated for both devices stressed at $V_{\rm gs} = V_{\rm ds}$ = 2.2 V and $V_{\rm gs}$ =

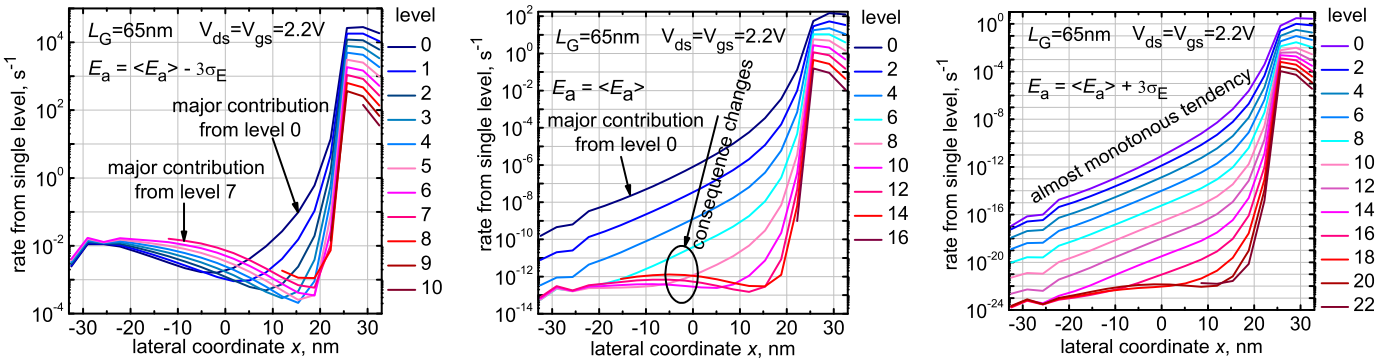

Fig. 6: The hydrogen release rates for different levels of the truncated harmonic oscillator. The data are plotted for the n-MOSFET with a 65 nm channel length subjected to stress at $V_{\rm ds} = V_{\rm gs}$ = 2.2 V. While calculating the cumulative dissociation rate, the dispersion of the activation energy is considered. Integration is performed in the range of $[\langle E_{\rm a}\rangle - 3\sigma_{\rm E}; \langle E_{\rm a}\rangle + 3\sigma_{\rm E}]$. The rates are computed for three fixed values: $E_{\rm a} = \langle E_{\rm a}\rangle - 3\sigma_{\rm E}$ (left), $E_{\rm a} = \langle E_{\rm a}\rangle$ (center), and $E_{\rm a} = \langle E_{\rm a}\rangle + 3\sigma_{\rm E}$ (right).

1.1 V, $V_{\rm gs}$ = 2.2 V, respectively, are plotted. The DFs are depicted at different positions in the device, i.e. with the coordinate varying from the source to the drain. To analyze the effect of electron-electron scattering, Fig. 2 also provides the DFs calculated disregarding EES. One can see that the DFs are severely non-equilibrium and demonstrate quite long high-energy tails, which suggest a high probability of the AB-mechanism. Second, the distributions calculated closer to the drain reveal rudiments of the Boltzmann distribution for low energies. Finally, electron-electron scattering substantially changes the shape of the functions, populating their high-energy tails. This results in pronounced humps at higher energies leading to high-energy tails of the DFs. This tendency is also reflected in Fig. 5 which summarizes the carrier acceleration integrals plotted as a function of the lateral coordinate x for both devices and for the same stress conditions as Fig. 2.

Fig. 6 shows dissociation rates from each vibrational level weighted with the level occupancy plotted for the 65 nm MOSFET and $V_{\rm gs}$ = $V_{\rm ds}$ = 2.2 V for three different values of the activation energy $E_{\rm a}$: $\langle E_{\rm a}\rangle - 3\sigma_{\rm E}$, $\langle E_{\rm a}\rangle$, and $\langle E_{\rm a}\rangle + 3\sigma_{\rm E}$. Note that since $E_{\rm a}$ varies according to a normal distribution these particular dissociation rates contribute to the total bond-breakage rate. It has been claimed [18] that in short-channel devices hydrogen release from the level with i=2 is dominant. Our results demonstrate, however, that due to the severe non-uniformity of the AI and the damage produced by hot-carrier stress the situation can be *substantially different along the interface*. In fact, for $E_{\rm a}$=$\langle E_{\rm a}\rangle - 3\sigma_{\rm E}$ the ground state provides only a minor contribution closer to source, while this contribution becomes prominent towards the drain.

Fig. 7 provides a summary of interface state density profiles $N_{\rm it}(x)$ calculated for the 65 nm MOSFET stressed at $V_{\rm ds} = V_{\rm gs}$ = 1.8 V for all stress time steps. These profiles are obtained by using the calibrated model and for comparison we have also plotted those $N_{\rm it}(x)$ that are computed by the model where one of the ingredients is switched off. The $N_{\rm it}(x)$ concentrations demonstrate a drain side maximum which is related to hot channel electrons typical for the drain area of the channel. Indeed, if we suppress the rate of the AB-mechanism (triggered by hot carriers) this maximum becomes weaker and narrower. In contrast, the $N_{\rm it}(x)$ profiles are only slightly affected near the source when the AB-process is ignored. This is because the source is a reservoir of thermalized carriers and the AB-mechanism is unlikely to be triggered.

If electron-electron scattering is deactivated, the trend is similar to the situation when the AB-process is ignored. For instance, the $N_{\rm it}$ drain maximum also becomes weaker. This totally correlates with the change of the shape of the carrier distribution functions (Fig. 2) and the acceleration integrals (Fig. 5). The reason is that EES makes carrier "hotter" which is reflected in humps pronounced in the high-energy tails of the DFs, see Fig. 2. Therefore, suppressing EES is equal to depopulating of the high energetical fraction of the particle ensemble, and hence to partial suppression of the AB-mechanism.

Ignoring the effect of the MVE-mechanism is most pronounced between the transistor source and center. Near the drain carriers are hot enough and bond dissociation events are predominantly triggered by solitary carriers without pre-heating of the bonds by the MVE-process. This is not the case in the rest of the device where excitation of bond vibrational modes becomes more important. Due to the same reasons, the effects of the interaction between the dipole moment of the bond and the electric field as well as of the activation energy dispersion on the $N_{\rm it}(x)$ profiles is also more prominent closer to the source. In both devices and for both stress conditions the electric field features a maximum close to the source, see Fig. 3. As a result, the $d \times E_{\rm ox}$ energy reduction is more prominent there, leading to the secondary maximum of the density of interface states $N_{\rm it}$ generated during stress, see Fig. 7. This maximum becomes more pronounced at longer stress times and can determine long-term HCD.

Finally, the model has been calibrated in order to represent the linear drain current degradation observed in both devices under various stress conditions. It is important to emphasize that the model uses the unique set of the model parameters. Fig. 8 shows the experimental $\Delta I_{\rm dlin}(t)$ dependencies plotted vs. the simulated ones as well as curves obtained neglecting

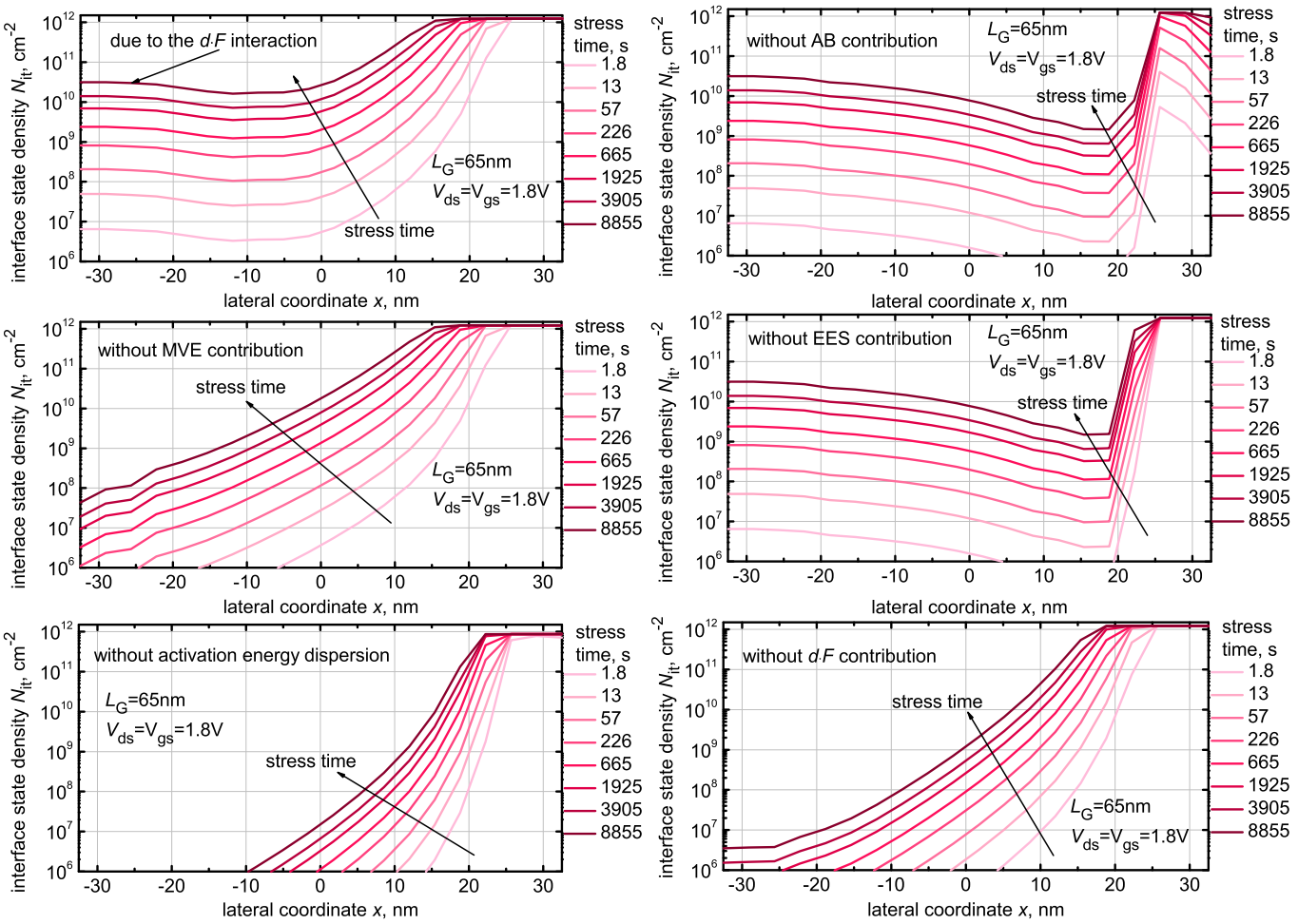

Fig. 7: The interface state density profiles $N_{\rm it}(x)$ ($L_{\rm G}$ = 65 nm, stress voltages: $V_{\rm ds}$ = $V_{\rm gs}$ = 1.8 V) calculated using the calibrated model regarding/disregarding one of the essential mechanisms: MVE- and AB-processes, EES, the dispersion of the activation energy for bond dissociation, and the reduction of this energy due to the interaction between the bond dipole moment and the electric field.

one of the model ingredients. One can see that in the 65 nm device *EES plays an important role in both stress regimes*, while in the 150 nm counterpart the effect of EES on $\Delta I_{\rm dlin}(t)$ characteristics is much less pronounced and even becomes negligible at $V_{\rm gs}$ =0.9 V, $V_{\rm gs}$ =1.8 V. Also, the role of the AB-mechanisms is important in all four cases. However, the discrepancy between the $\Delta I_{\rm dlin}(t)$ curves simulated with/without the AB-process decreases with stress time. This is because near the drain all available passive bonds are broken, $N_{\rm it}$ has reached the maximum level of N_0 and HCD is thus saturated. Increasing of the AB-process contribution is now related to the propagation of the front of the saturated $N_{\rm it}$ towards the source, which is a relatively slow process.

In contrast, hot-carrier degradation at long stress times is defined by the MVE-process and by the energy reduction due to the interaction of the bonds with the electric field. For instance, one can see that the distance between $\Delta I_{\rm dlin}(t)$ curves simulated regarding and ignoring the $d \times E_{\rm ox}$ energy reduction grows with time. Such a growth is due to the source $N_{\rm it}$ peak which strengthens with the stress time. Finally, ignoring the activation energy dispersion results in a dramatic underestimation of HCD at all stress times.

V. Conclusion

We have presented and validated the *first physical model for HCD which can capture both short- and long-channel devices* operating within a single set of the model parameters. The model arranges the entire hierarchy of phenomena involved into hot-carrier degradation starting at the microscopic level of defect generation and linking it via carrier transport with the device physics level. Our model is implemented in the deterministic Boltzmann transport equation solver ViennaSHE and covers all HCD sub-problems within the same modeling framework. The model provides consistent treatment of processes triggered by hot (AB-mechanism) and colder carriers (MVE-process). These processes are naturally considered as competing pathways of the same bond dissociation reaction.

Such model ingredients as AB- and MVE-mechanisms, EES, dispersion of the activation energy, and its variation due to the interaction of the Si-H bond with the electric field are shown to be essential and important. The AB-process – which is triggered by hot carriers – was demonstrated to

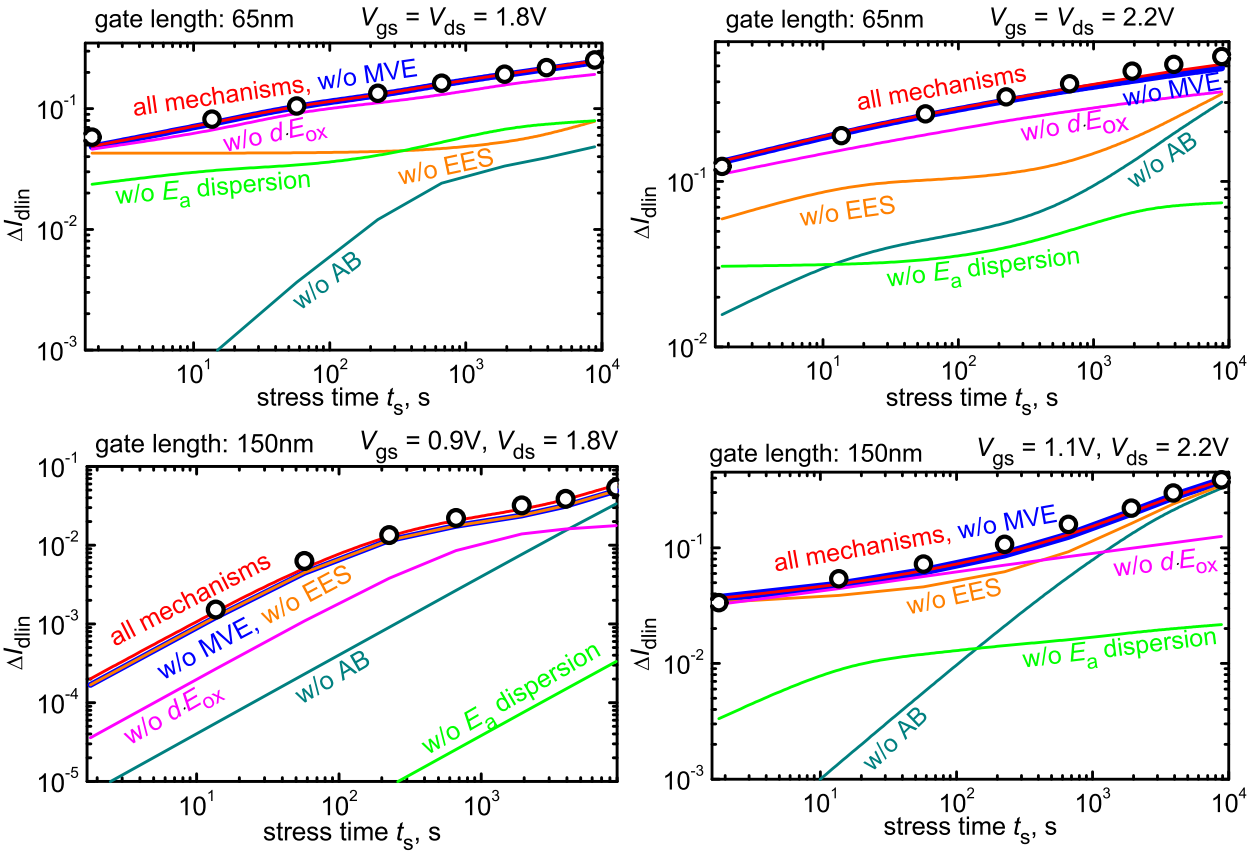

Fig. 8: The linear drain current ΔI_{dlin} change as a function of stress time: experiment vs. simulations. MOSFETs with channel lengths of 65 (two upper panels) and 150 nm (lower panels) have been stressed at worst-case conditions at T = 298 K and V_{ds} = 1.8 and 2.2 V, respectively. With all ingredients included the model represents the experimental $\Delta I_{\mathrm{dlin}}(t)$ curve. For comparison, $\Delta I_{\mathrm{dlin}}(t)$ simulated without the EES, AB-, MVE-mechanisms, activation energy dispersion, and its reduction due to the interaction of the dipole moment with electric field are plotted. One can see that EES plays a significant role in the case of L_{G} = 65 nm but is important or even negligible for L_{G} = 150 nm.

be important even in the short-channel devices if the stress voltages are relatively high. Electron-electron scattering is extremely important for short-channel devices while its impact was less pronounced in long-channel counterparts. Also, the role of EES becomes less prominent at longer stress times. Instead, such mechanisms as excitation of the multiple vibrational modes of the bond and interaction between the electric field and the bond dipole moment are responsible for HCD at longer stress times. Finally, our model agrees very well with experimental data at different channel lengths, making it a *good choice for predictive device optimization*.

Acknowledgment

The authors acknowledge support by the Austrian Science Fund (FWF), grants P23598 and P26382, and the European Community FP7 projects N° 261868 (MORDRED) and 619246 (ATHENIS_3D).

References

[1] W. McMahon, K. Matsuda, J. Lee, K. Hess, and J. Lyding, "The Effects of a Multiple Carrier Model of Interface States Generation of Lifetime Extraction for MOSFETs," in *Proc. Int. Conf. Mod. Sim. Micro*, vol. 1, 2002, pp. 576–579.

[2] A. Bravaix and V. Huard, "Hot-Carrier Degradation Issues in Advanced CMOS Nodes," in *Proc. European Symposium on Reliability of Electron Devices Failure Physics and Analysis (ESREF), tutorial*, 2010.

[3] S. Rauch, F. Guarin, and G. La Rosa, "High-V_{gs} PFET DC Hot-carrier Mechanism and its Relation to AC Degradation," *IEEE Trans. Dev. Material Reliab.*, vol. 10, no. 1, pp. 40–45, 2010.

[4] S. Tyaginov, I. Starkov, O. Triebl, H. Enichlmair, C. Jungemann, J. Park, H. Ceric, and T. Grasser, "Secondary Generated Holes as a Crucial Component for Modeling of HC Degradation in High-voltage n-MOSFET," in *Proc. International Conference on Simulation of Semiconductor Processes and Devices (SISPAD)*, 2011, pp. 123–126.

[5] S. Tyaginov and T. Grasser, "Modeling of Hot-Carrier Degradation: Physics and Controversial Issues," in *Proc. International Integrated Reliability Workshop (IIRW)*, 2012, pp. 206–215.

[6] C. Hu, S. Tam, F. Hsu, P.-K. Ko, T.-Y. Chan, and K. Terrill, "Hot-electron-induced MOSFET Degradation Model, Monitor and Improvement," *IEEE Trans. Electron Dev.*, vol. 48, no. 4, pp. 375–385, 1985.

[7] B. Doyle, M. Bourcerie, C. Bergonzoni, R. Benecchi, A. Bravis, K. Mistry, and A. Boudou, "The Generation and Characterization of Electron and Hole Traps Created by Hole Injection During Low Gate Voltage Hot-Carrier Stressing of n-MOS Transistors," *IEEE Trans. Electron Dev.*, vol. 37, no. 8, pp. 1869–1876, 1990.

[8] J.-S. Goo, Y.-G. Kim, H. Lee, H.-Y. Kwon, and H. Shin, "An Analytical Model for Hot-carrier-induced Degradation of Deep-submicron n-channel LDD MOSFETs," *Solid-State Electron.*, vol. 38, no. 6, pp. 1191–1196, 1995.

[9] P. Childs and C. Leung, "New Mechanism of Hot Carrier Generation in Very Short Channel MOSFETs," *Electronics Lett.*, vol. 31, no. 2, pp. 139–141, 1995.

[10] S. Rauch, F. Guarin, and G. La Rosa, "Impact of E-E Scattering to the Hot Carrier Degradation of Deep Submicron NMOSFETs," *IEEE Electron Dev. Lett.*, vol. 19, no. 12, pp. 463–465, 1998.

[11] S. Rauch and G. L. Rosa, "CMOS Hot Carrier: From Physics to End Of Life Projections, and Qualification," in *Proc. International Reliability Physics Symposium (IRPS), tutorial*, 2010.

[12] K. Hess, L. Register, B. Tuttle, J. Lyding, and I. Kizilyalli, "Impact of Nanostructure Research on Conventional Solid-State Electronics: the Giant Isotope Effect in Hydrogen Desorption and CMOS Lifetime," *Physica E*, vol. 3, pp. 1–7, 1998.

[13] T. Mizuno, A. Toriumi, M. Iwase, M. Takanashi, H. Niiyama, M. Fukmoto, and M. Yoshimi, "Hot-carrier Effects in 0.1μm Gate Length CMOS Devices," in *Proc. International Electron Devices Meeting (IEDM)*, 1992, pp. 695–698.

[14] W. McMahon, A. Haggag, and K. Hess, "Reliability Scaling Issues for Nanoscale Devices," *IEEE Trans. Nanotech.*, vol. 2, no. 1, pp. 33–38, 2003.

[15] A. Bravaix, C. Guerin, V. Huard, D. Roy, J. Roux, and E. Vincent, "Hot-carrier Acceleration Factors for Low Power Management in DC-AC Stressed 40nm NMOS Node at High Temperature," in *Proc. International Reliability Physics Symposium (IRPS)*, 2009, pp. 531–546.

[16] S. Rauch and G. L. Rosa, "The Energy Driven Paradigm of NMOSFET Hot Carrier Effects," in *Proc. International Reliability Physics Symposium (IRPS)*, 2005.

[17] Y. Randriamihaja, V. Huard, X. Federspiel, A. Zaka, P. Palestri, D. Rideau, and A. Bravaix, "Microscopic Scale Characterization and Modeling of Transistor Degradation Under HC Stress," *Microel. Reliab.*, vol. 52, no. 11, pp. 2513–2520, 2012.

[18] Y. Randriamihaja, X. Federspiel, V. Huard, A. Bravaix, and P. Palestri, "New Hot Carrier Degradation Modeling Reconsidering the Role of EES in Ultra Short n-channel MOSFETs," in *Proc. International Reliability Physics Symposium (IRPS)*, 2013, pp. 1–5.

[19] C. Guerin, V. Huard, and A. Bravaix, "The Energy-Driven Hot-carrier Degradation Modes of nMOSFETs," *IEEE Trans. Dev. Material. Reliab.*, vol. 7, no. 2, pp. 225–235, 2007.

[20] M. Bina, K. Rupp, S. Tyaginov, O. Triebl, and T. Grasser, "Modeling of Hot Carrier Degradation Using a Spherical Harmonics Expansion of the Bipolar Boltzmann Transport Equation," in *Proc. International Electron Devices Meeting (IEDM)*, 2012, pp. 713–716.

[21] S. Tyaginov, I. Starkov, O. Triebl, J. Cervenka, C. Jungemann, S. Carniello, J. Park, H. Enichlmail, C. Kernstock, E. Seebacher, R. Minixhofer, H. Ceric, and T. Grasser, "Interface Traps Density-of-states as a Vital Component for Hot-carrier Degradation Modeling," *Microelectronics Reliability*, vol. 50, pp. 1267–1272, 2010.

[22] E. Li, E. Rosenbaum, J. Tao, G.-F. Yeap, M. Lin, and P. Fang, "Hot-carrier Effects in nMOSFETs in 0.1 μm cmos technology," in *Proc. International Reliability Physics Symposium (IRPS)*, 1999, pp. 253–258.

[23] K. Rupp, T. Grasser, and A. Jungel, "On the Feasibility of Spherical Harmonics Expansions of the Boltzmann Transport Equation for Three-Dimensional Device Geometries," in *Proc. International Electron Devices Meeting (IEDM)*, 2011, pp. 789–792.

[24] J. Bude and K. Hess, "Thresholds of Impact Ionization in Semiconductors," *Journal of Applied Physics*, vol. 72, no. 8, pp. 3554–3561, 1992.

[25] A. Stesmans, "Revision of H_2 Passivation of P_2 Interface Defects in Standard (111)Si/SiO_2," *Applied Physics Letters*, vol. 68, no. 19, pp. 2723–2725, 1996.

[26] ——, "Passivation of P_{b0} and P_{b1} Interface Defects in Thermal (100) Si/SiO_2 with Molecular Hydrogen," *Appl. Phys. Lett.*, vol. 68, no. 15, pp. 2076–2078, 1996.

[27] G. Pobegen, S. Tyaginov, M. Nelhiebel, and T. Grasser, "Observation of Normally Distributed Activation Energies for the Recovery from Hot Carrier Damage," *IEEE Electron Dev. Lett.*, vol. 34, no. 8, pp. 939–941, 2013.

[28] J. McPherson, "Quantum Mechanical Treatment of Si-O Bond Breakage in Silica Under Time Dependent Dielectric Breakdown Testing," in *Proc. International Reliability Physics Symposium (IRPS)*, 2007, pp. 209–216.

[29] C. Guerin, V. Huard, and A. Bravaix, "General Framework about Defect Creation at the Si/SiO_2 Interface," *Journ. Appl. Phys.*, vol. 105, pp. 114 513–1–114 513–12, 2009.

[30] A. Haggag, W. McMahon, K. Hess, K. Cheng, J. Lee, and J. Lyding, "High-performance Chip Reliability from Short-time-tests. Statistical Models for Optical Interconnect and HCI/TDDB/NBTI Deep-Submicron Transistor Failures," in *Proc. International Reliability Physics Symposium (IRPS)*, 2001, pp. 271–279.

[31] K. Hess, A. Haggag, W. McMahon, K. Cheng, J. Lee, and J. Lyding, "The Physics of Determining Chip Reliability," *Circuits and Devices Mag.*, pp. 33–38, 2001.

[32] V. Huard, M. Denais, and C. Parthasarathy, "NBTI Degradation: From Physical Mechanisms to Modelling," *Microel. Reliab.*, vol. 46, no. 1, pp. 1–23, 2006.